Article

Model of Growth Cone Membrane Polarization via Microtubule Length Regulation

Bin Xu[1] and Paul C. Bressloff[1,*]
[1]Mathematics, University of Utah, Salt Lake City, Utah

ABSTRACT   We present a mathematical model of membrane polarization in growth cones. We proceed by coupling an active transport model of cytosolic proteins along a two-dimensional microtubule (MT) network with a modified Dogterom-Leibler model of MT growth. In particular, we consider a Rac1-stathmin-MT pathway in which the growth and catastrophe rates of MTs are regulated by cytosolic stathmin, while the stathmin is regulated by Rac1 at the membrane. We use regular perturbation theory and numerical simulations to determine the steady-state stathmin concentration, the mean MT length distribution, and the resulting distribution of membrane-bound proteins. We thus show how a nonuniform Rac1 distribution on the membrane generates a polarized distribution of membrane proteins. The mean MT length distribution and hence the degree of membrane polarization are sensitive to the precise form of the Rac1 distribution and parameters such as the catastrophe-promoting constant and tubulin association rate. This is a consequence of the fact that the lateral diffusion of stathmin tends to weaken the effects of Rac1 on the distribution of mean MT lengths.

INTRODUCTION

During neural development, the growth cone of an axon has to respond accurately to extracellular chemical gradients that direct and steer its growth. Chemoattractants (chemorepellents) are detected by receptors in the growth cone membrane, which trigger signaling cascades that lead to the restructuring of the cytoskeleton and growth toward (away from) the stimulus. The growth cone cytoskeleton consists of microtubules (MTs) within a central (C) domain and actin filaments within the peripheral (P) domain (1) (Fig. 1). The MTs provide the structural backbone of the axonal shaft and a substrate for intracellular transport to the growth cone. They polymerize with their growing ends pointed toward the leading edge of the growth cone. Actin filaments within the P-domain form the filopodia and lamellipodia that shape and direct the motility of the growth cone. In both structures, the actin filaments face with their barbed (growing) ends toward the plasma membrane. Polymerization of actin filaments toward the leading edge causes the extension and protrusion of the growth cone. This creates a force that pushes the actin network and the tightly linked plasma membrane backward (retrograde flow), and hinders the invasion of the MTs into the P-domain. The retrograde flow is also enhanced by the action of myosin molecular motors, which drag the actin cytoskeleton back toward the C-domain where actin filaments depolymerize at their pointed ends. If there is a balance between actin polymerization in the P-domain and retrograde flow, then there is no elongation. However, signals

from surface adhesion receptors bound to a substrate can suppress the retrograde flow of actin filaments, shifting the balance toward polymerization-driven forward motion that involves both actin filaments and microtubules.

It used to be thought that the actin cytoskeleton was the main driver of changes in cell shape during neuronal morphogenesis, with MTs playing a secondary role. However, in recent years it has become clear that MTs also actively participate in the restructuring of cell shape (2-4). The latter occurs via the regulation of MT lengths by a variety of signaling proteins. Some of these proteins act directly on the MTs, affecting their rates of growth, whereas others indirectly control MT lengths by sequestering tubulin. To understand the potential targets of regulatory proteins, we briefly review some properties of MTs. During assembly, heterodimers of α-tubulin and β-tubulin bind head-to-tail to form polarized protofilaments with different rates of polymerization at the two ends: a faster growing plus-end capped by β-subunits and a slower minus-end capped by α-subunits. It has been observed experimentally that MTs undergo a process of dynamic instability, in which they randomly switch between growing and shrinking phases (5). Such an instability can be characterized in terms of the rate of polymerization and depolymerization, and the frequencies of catastrophes (transitions from polymerization to depolymerization) and rescues (transitions from depolymerization to polymerization) (6). All of these processes depend on tubulin-bound GTP hydrolysis that occurs during microtubule assembly and destabilizes the growing filament after polymerization.

One important family of soluble phosphoproteins found in growth cones that can regulate MT growth is stathmin (7-9). It is known that stathmin can indirectly inhibit MT
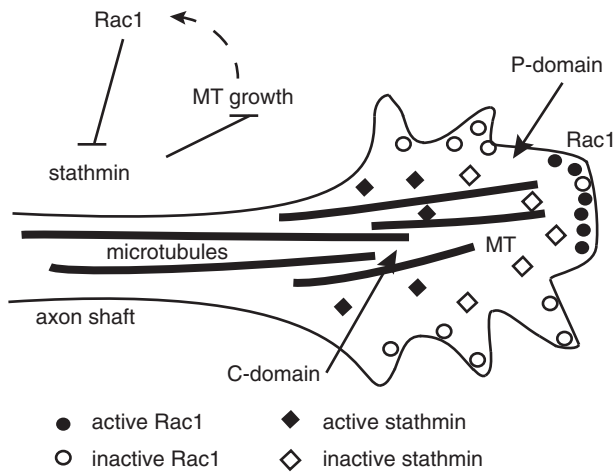
FIGURE 1 Sketch of the Rac1-stathmin-MT pathway. Rac1 proteins (*circles*) are located at the leading edge of the growth cone in active (*solid circles*) or inactive form (*open circles*). The active region of Rac1 generates a gradient in stathmin phosphorylation such that the concentration of active stathmin increases with distance from the active Rac1 domain. Active stathmin inhibits the growth of MTs. There is also a potential feedback pathway involving the interaction between Rac1 and MT tips, which we neglect in our model.

growth by sequestering tubulin, thus lowering the local tubulin concentration, reducing the MT growth velocity, and increasing the catastrophe rate (10,11). There is also experimental evidence of an alternative mechanism for reducing the MT growth rate, which occurs at high pH values, in which stathmin increases the MT catastrophe rate, but not the growth velocity, by direct interaction with the MT filaments (12). Stathmin itself can be regulated through a Rac1-Pak pathway (11) (Fig. 1). The signaling molecule Rac1 is a GTPase of the Rho family that is found to be active (phosphorylated) when membrane-bound at the leading edge of the growth cone (13). Active Rac1 can deactivate stathmin via the intermediate protein Pak (14). Moreover, because the active form of Rac1 is located at the leading edge of the growth cone, it can induce a spatial gradient of stathmin phosphorylation and thus stathmin MT/tubulin interactions (15). Finally, because the distribution of active Rac1 within the leading edge can be modified by extracellular guidance cues (16), it follows that the Rac1-stathmin-MT pathway provides one possible mechanism for growth cone steering via MT polarization.

The above mechanism has been explored in a computational model of a two-dimensional (2D) growth cone by Mahajan and Athale (17). These authors consider a reaction-diffusion model of receptor-driven activation (dephosphorylation) and inactivation (phosphorylation) of stathmin, and modulate the MT dynamics by increasing the local catastrophe rate according to the local stathmin concentration. (They also take into account forces arising from the retrograde pushing of MTs by actin.) One major conclusion of their study is that the stathmin-based regulation of MT dynamics is sufficient to generate growth-cone turning, without the need for amplification from positive feedback in which MT tips promote the inactivation of stathmin. Indeed, their modeling study suggests that the feedback from MTs can amplify noise and generate spurious polarization in the absence of external cues. Recently, Zeitz and Kierfeld (18) have analyzed a more biophysically detailed model of MT regulation based on the signaling proteins Rac1 and stathmin. In contrast to the 2D growth cone model of Mahajan and Athale (17), they consider a one-dimensional (1D) model consisting of an ensemble of parallel MTs growing within a 1D concentration gradient of stathmin. The latter is generated by the Rac1-based dephosphorylation of stathmin at one end of the domain. Zeitz and Kierfeld (18) consider both catastrophe-promoting and tubulin-sequestering mechanisms of stathmin regulation, and find that the latter exhibits a stronger dependence on the level of active Rac1. Moreover, the inclusion of feedback between MT tips and activation of Rac1 has a much more significant effect on the tubulin-sequestering mechanism, resulting in bistability between a state of high Rac1 activation and a state of low Rac1 activation.

In this article, we consider a different aspect of growth cone steering via MT polarization, namely, how a nonuniform distribution of MT lengths generated by the Rac1-stathmin-MT pathway can support membrane polarization in the leading edge of the growth cone. Under the assumption that all MTs are nucleated from the same source, a variation in MT length translates into a variation in the distance of MT plus-ends from the trailing edge of the growth cone. The latter causes a corresponding nonuniformity in the active transport of signaling proteins (or lipids) along the MT filament tracks, resulting in a nonuniform distribution of membrane-associated molecules. The latter result is of course not surprising—the point of our modeling study is to determine whether the mechanism of MT regulation considered by previous authors is sufficient to generate a significant variation in the concentration of membrane-bound molecules. To compare the tubulin-sequestering and catastrophe-promoting mechanisms of stathmin-based MT regulation, we adopt the model of Zeitz and Kierfeld (18). A major result of our modeling study is to establish that only the tubulin-sequestering mechanism appears to support a significant variation in membrane-bound proteins, and this is sensitive to the precise form of the Rac1 distribution and parameters such as the tubulin association rate. This is partly due to the fact that the lateral diffusion of stathmin within the growth cone reduces the spatial variation of MT lengths compared to the results of the 1D model considered by Zeitz and Kierfeld (18).

Note that our model differs from previous studies of the role of active transport in cell polarization, which consider spatial inhomogeneities in the density of MTs in axons (19,20) or actin filaments in budding yeast (21-24). That is, all filaments are assumed to reach the membrane surface. In the case of budding yeast, the actin filaments actually nucleate from the membrane, and the density of filaments

is regulated by the active, membrane-bound form of the Rho GTPase Cdc42. Because Cdc42 is itself actively transported by myosin motors along the actin network, there is a positive feedback loop that can reinforce spatial asymmetries, resulting in spontaneous cell polarization (21). However, the mechanism in growth cones appears to be different, because MTs nucleate in the cell body, and it is asymmetries in the degree of penetration of MTs into the peripheral zone that contributes to cell polarization.

MATERIALS AND METHODS

In this section, we present the various components of the model. Note that the novel component, to our knowledge, is the active transport model, which we then couple to a 2D version of the stathmin-MT model of Zeitz and Kierfeld (18). A list of parameters and their values used in our numerical results is provided in Table 1, where we also give references to the supporting literature. The parameter values for the stathmin-MT components are basically as in Zeitz and Kierfeld (18).

Active transport model

Our model treats the growth cone as a rectangular 2D domain $\{(x,z); 0 \leq x \leq L, 0 \leq z \leq R\}$ with the leading edge of the growth cone at $z = R$ and the MTs parallel to the z axis (Fig. 2) Based on experimental measurements

TABLE 1 Parameter values used for simulations

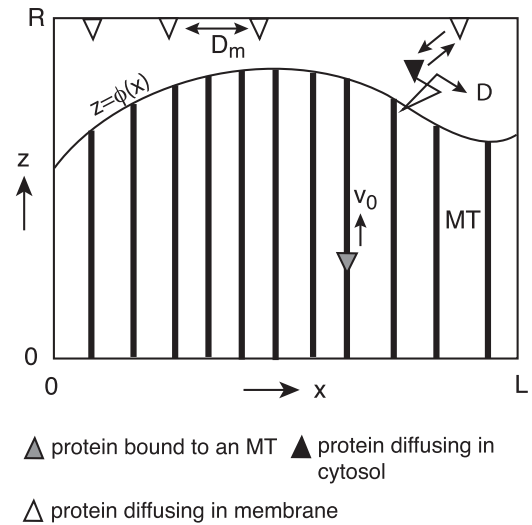| Description	Parameter	Value (Reference)
Time step	Δt	0.01 s
Spatial step	Δx	0.1 μm
Growth cone		
Width	L	10 μm
Depth	R	10 μm
Cell edge region	δ	0.02 μm
Active-transport model		
Diffusion coefficient	D	0.1 μm^2/s (19)
Diffusion coefficient(membrane)	D_m	0.01 μm^2/s (19)
Advection coefficient	v_0	1 μm/s
Detachment rate	k_-	0.1/s (19)
Attachment rate	k_+	1 μm/s (19)
Microtubule		
Tubulin concentration	$[T_0]$	19.4 μM
Effective dimer length	d	0.6 nm
Tubulin associate rate	$\omega_{on} = \kappa_{on}[T_0]$	143/s (25)
Dissociation velocity	$\kappa_{off}d$	3.6 nm/s (26)
Growth velocity ($S_{on} = 0$)	v_+	0.06 μm/s (25-28)
Shrinkage velocity	v_-	0.18 μm/s (25,27,28)
Rescue rate	ω_r	0.18/s (25,29,30)
Catastrophe rate ($S_{on} = 0$)	ω_c	0.0007/s
Catastrophe rate	a	20 s
($\omega_c = 1/(a + bv_+)$)	b	1.38×10^{10} s^2/m (31)
Stathmin		
Activation rate	k_{on}	1/s (15)
Deactivation rate	k_{off}	300/s
Diffusion coefficient	D_s	15 μm^2/s (15)
Sequestering equilibrium constant	K_0	25/μM^2 (10,15,32-34)
Catastrophe promotion constant	k_c	0.005 s^{-1} μM^{-1} (35)

FIGURE 2 A simplified 2D model of a growth cone with a nonuniform distribution of MT lengths as specified by the interface $z = \phi(x)$. The boundary $z = R$ represents the membrane at the leading edge of the growth cone. When a protein is bound to a MT via a molecular motor, it moves at speed v_0 toward the leading edge. For simplicity, we do not explicitly model the vesicular nature of active motor transport. A cytosolic protein diffuses when unbound from a MT with diffusivity D, and can bind/unbind to the leading edge at a rate $k_\pm$. Membrane-bound protein undergoes lateral diffusion with diffusivity D_m.

of growth cones of cultured neurons, we take $L = R = 10$ μm (36). We assume that the MTs form a uniformly distributed bundle of filaments orthogonal to the leading edge. Let $\phi(x)$ denote the mean distance of the plus-ends of the local MT population at x from the leading edge—the corresponding mean length is $\phi(x)$. (The resulting interface $z = \phi(x)$ need not be continuous.) Suppose that a given configuration of MTs acts as a system of filament tracks for the active transport of some signaling protein that is targeted for delivery to the leading edge of the growth cone. (In this article, we leave the identity of the actively transported cytosolic molecules open, but candidates are signaling proteins such as Cdc42 and Rac1 or membrane lipids; see the Discussion.) Let $c(x,z,t)$ denote the concentration of the signaling protein within the cytosol of the growth cone and $u(x,t)$ denote the concentration at the leading edge. The protein molecules in the cytosol undergo alternating sequences of diffusion and active transport by molecular motors along microtubules while molecules at the membrane undergo diffusion along the membrane. At the leading edge $z = R$, molecules can attach and detach from the membrane with rates k_+ and k_-, respectively. The concentrations $c(x,z,t)$ and $u(x,t)$ evolve according to the advection-diffusion equations (note that the use of advection-diffusion equations to model active intracellular transport can be justified from first-principles under certain assumptions regarding the rates of switching between different motile states of a motor-cargo complex (37-40)):

$$\frac{\partial c(x,z,t)}{\partial t} = -v(x,z)\frac{\partial c(x,z,t)}{\partial z} + D\frac{\partial^2 c(x,z,t)}{\partial x^2} + D\frac{\partial^2 c(x,z,t)}{\partial z^2}, \tag{1a}$$

$$\frac{\partial u(x,t)}{\partial t} = D_m\frac{\partial^2 u(x,t)}{\partial x^2} + k_+c(x,R,t) - k_-u(x,t), \tag{1b}$$

where

$$v(x,z) = \begin{cases} v_0, & \text{if } 0 < z < \phi(x), \\ 0, & \text{if } \phi(x) < z < R. \end{cases} \quad (2)$$

Here the velocity $v(x,z)$ has a jump discontinuity at the interface $\Gamma = \{(x,z), z = \phi(x)\}$. Equations 1a and 1b are supplemented by the reflecting boundary conditions at $x = 0, L$ and $z = 0$,

$$\frac{\partial c}{\partial x}(0,z,t) = \frac{\partial c}{\partial x}(L,z,t) = 0,$$
$$\frac{\partial u}{\partial x}(0,t) = \frac{\partial u}{\partial x}(L,t) = 0, \quad (3)$$

$$D\frac{\partial c}{\partial z}(x,0,t) - v_0 c(x,0,t) = 0,$$
$$0 < x < L, \quad (4)$$

and a flux conservation condition at $z = R$

$$-D\frac{\partial c}{\partial z}(x,R,t) = k_+ c(x,R,t) - k_- u(x,t),$$
$$0 < x < L. \quad (5)$$

At the interface $\Gamma = \{(x,z), z = \phi(x)\}$, we impose continuity of $c(x,z,t)$ and the corresponding flux, which leads to the jump conditions

$$c(x,z,t)\Big|_{z=\phi_-(x)}^{z=\phi_+(x)} = 0,$$
$$\left[v(x,z)c(x,z,t) - D\frac{\partial c(x,z,t)}{\partial z}\right]\Big|_{z=\phi_-(x)}^{z=\phi_+(x)} = 0, \quad (6)$$

where $\phi_\pm = \lim_{\epsilon \to 0}[\phi \pm \epsilon], \epsilon > 0$.

One simplification of the above model is that it ignores the vesicular nature of active transport (see also Hawkins et al. (19), Bressloff and Xu (20), and Marco et al. (22)). That is, we effectively model transport in terms of a continuous flux of molecules. However, as highlighted by Layton et al. (23), vesicular transport of signaling proteins makes cell polarization more difficult to sustain. To begin, it is clear that if the concentration of signaling molecules within a vesicle is the same as a local region of membrane, then fusion of the vesicle releases both signaling molecules and additional lipid membrane so the concentration does not change, in contrast to a continuous flux of signaling molecules alone. This implies that exocytic vesicles need to have higher concentrations of the signaling molecule than the polarization site to enhance the concentration. A dynamic equilibrium of recycling can only be maintained if endocytic vesicles also have an enhanced concentration of signaling molecules. There are various active mechanisms for enhancing the concentration of proteins within vesicular membranes, such as the interactions of soluble *n*-ethylmaleimide-sensitive factor attachment protein receptors (41), and we will assume that this occurs in the growth cone. (Although evidence for such processes within the context of growth cone polarization is lacking as of this writing, it has recently been observed that vesicles deliver Cdc42 to sites of polarized growth in yeast (42).) Finally, note that this issue does not apply to the transport of plasma membrane itself. Indeed, there is growing evidence that a shift in the balance between endocytosis and exocytosis for membrane trafficking contributes to growth cone steering, by increasing (decreasing) the local amount of plasma membrane in the vicinity of a chemoattractant (chemorepellent) (43). Such a process depends on an asymmetric elevation of cytosolic Ca^{2+} across the growth cone.

Stathmin-regulated MT growth model

The main aim of our article is to calculate the steady-state concentration of membrane-bound signaling proteins for an interface Γ determined by a stathmin-based model of MT polarization. We proceed by constructing a 2D version of the reaction-diffusion model of Zeitz and Kierfeld (18), in which there is a fixed distribution of Rac1 in the leading edge of the growth cone, and feedback interactions between Rac1 and MT tips that reach the membrane are ignored. The basic assumptions of the stathmin-regulated MT growth model are thus as follows (see Fig. 3):

1) The concentration of active Rac1 in the leading edge is given by the prescribed function $r_{on}(x)$, $0 \leq X \leq L$.
2) Stathmins in both the active (dephosphorylated) and inactive (phosphorylated) states diffuse in the cytosol with the same diffusion coefficient D. Activation of stathmin takes place in the cytosol with a constant rate k_{on} while deactivation only occurs at the leading edge under the regulation of the active Rac1 at a rate k_{off}.
3) MTs stochastically switch between a growth state and a shrinkage state at a catastrophe rate ω_c and a rescue rate ω_r. MTs polymerize in the positive z direction at an average velocity v_+ in the growth state and depolymerize at an average velocity $-v_-$ in the shrinkage state with $v_\pm > 0$.
4) The growth of MTs is regulated by the local stathmin concentration either by directly increasing the catastrophe rate or by sequestering tubulin (see below).

MT catastrophe model

Let $p_\pm(x,z,t)$ denote the density of MTs at lateral position x at time t with length z and in the growth (+) or shrinkage (−) phase. Here length is determined by the vertical distance z of an MT's plus-end from the trailing edge of the growth cone at $z = 0$. The densities $p_\pm$ evolve according to the extended Dogterom-Leibler model (6),

$$\frac{\partial p_+}{\partial t}(x,z,t) = -\frac{\partial[v_+(x,z,t)p_+(x,z,t)]}{\partial z}$$
$$- \omega_c(x,z,t)p_+(x,z,t) + \omega_r p_-(x,z,t), \quad (7a)$$

$$\frac{\partial p_-}{\partial t}(x,z,t) = v_-\frac{\partial p_-(x,z,t)}{\partial z} + \omega_c(x,z,t)p_+(x,z,t)$$
$$- \omega_r p_-(x,z,t), \quad (7b)$$
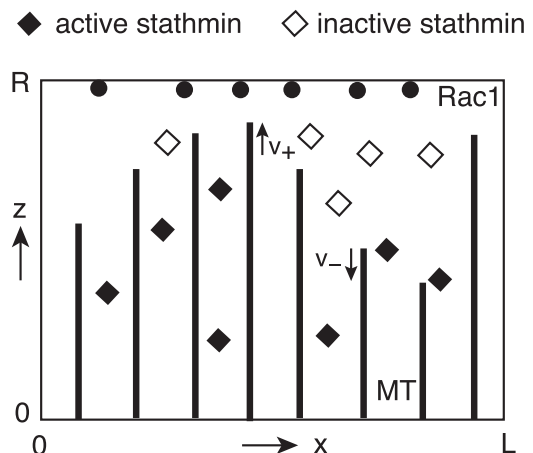
◆ active stathmin ◇ inactive stathmin

FIGURE 3 2D stathmin-regulated MT growth model. Active Rac1 in the leading edge ($z = R$) generates a gradient of phosphorylated stathmin. As z decreases, the concentration of active (dephosphorylated) stathmin becomes larger, thus increasing the likelihood that an MT undergoes catastrophe.

where the space-time dependence of the catastrophe rate ω_c and growth velocity v_+ arises from their dependence on the stathmin concentration, see below. We impose reflecting boundary conditions at $x = 0, L$,

$$\frac{\partial p_\pm}{\partial x}(x, z, t)\bigg|_{x=0,L} = 0, \qquad (8)$$

and at $z = 0, R$,

$$v_+(x,0)p_+(x,0,t) - v_- p_-(x,0,t)$$
$$= v_+(x,R)p_+(x,R,t) - v_- p_-(x,R,t) = 0. \qquad (9)$$

Stathmin model

Let $S_{on}(x,z,t)$ and $S_{off}(x,z,t)$ denote the concentration of active and inactive stathmin, respectively, at position (x,z) at time t. The stathmin concentrations are taken to satisfy the reaction-diffusion equations

$$\frac{\partial S_{off}}{\partial t}(x,z,t) = D_s \nabla^2 S_{off}(x,z,t) - k_{on} S_{off}(x,z,t), \qquad (10a)$$

$$\frac{\partial S_{off}}{\partial t}(x,R,t) = -\frac{D_s}{\delta} \frac{\partial S_{off}}{\partial z}\bigg|_{z=R} - k_{on} S_{off}(x,R,t)$$
$$+ r_{on}(x)k_{off} S_{on}(x,R,t), \qquad (10b)$$

and

$$\frac{\partial S_{on}}{\partial t}(x,z,t) = D_s \nabla^2 S_{on}(x,z,t) + k_{on} S_{off}(x,z,t), \qquad (11a)$$

$$\frac{\partial S_{on}}{\partial t}(x,R,t) = -\frac{D_s}{\delta} \frac{\partial S_{on}}{\partial z}\bigg|_{z=R} + k_{on} S_{off}(x,R,t)$$
$$- r_{on}(x)k_{off} S_{on}(x,R,t). \qquad (11b)$$

(Note that models for a spatially separated kinase/phosphatase cycle similar to the stathmin model have been developed by a number of authors; see, for example, Brown and Kholodenko (44) and Lipkow and Odde (45).) Following Zeitz and Kierfeld (18), we are assuming that there exists a boundary layer of width δ at the leading edge $z = R$, within which stathmin molecules deactivate (phosphorylate) at a rate $r_{on}(x)k_{off}$ and activate (dephosphorylate) at a rate k_{on}. Outside this boundary layer, only dephosphorylation occurs. Eqs. 10 and 11 are supplemented by the following boundary conditions at $x = 0, L$ and $z = 0$:

$$\frac{\partial S_{off,on}}{\partial x}\bigg|_{x=0,L} = 0,$$
$$\frac{\partial S_{off,on}}{\partial z}\bigg|_{z=0} = 0. \qquad (12)$$

The stathmin model is coupled to the MT growth model by taking the catastrophe rate, and possibly the growth velocity, to depend on the local concentration of active stathmin. We consider two forms of coupling (18):

1) One suggested pathway for stathmin to suppress MT growth is by direct interaction with an MT filament, resulting in an increase in the catastrophe rate. Experimental data suggests a linear increase of the catastrophe rate with the concentration of active stathmin, so we take

$$\omega_c(x,z,t) = \omega_c^0 + k_c S_{on}(x,z,t), \qquad (13)$$

with $k_c = 0.005 \text{ s}^{-1} \mu M^{-1}$ and $\omega_c^0 = 7 \times 10^{-4} \text{ s}^{-1}$ (35).

2) Another possible pathway is via sequestering of tubulin. It turns out that a single active stathmin protein sequesters two tubulin proteins (35),

$$2T + S \rightleftharpoons ST_2.$$
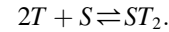
If this is combined with the kinetics of activation/deactivation of stathmin, then at chemical equilibrium, the normalized concentration of free tubulin $t \equiv [T]/[T_0]$, where $[T_0]$ is the total tubulin concentration, can be expressed as a nonlinear function of the normalized active stathmin concentration $s_{on} = S_{on}/[T_0]$ (18),

$$t(s_{on}) = \frac{1}{3}\left[1 - 2s_{on} + \frac{k(1 - 2s_{on})^2 - 3}{k\alpha(s_{on})} + \alpha(s_{on})\right],$$

with $k \equiv K_0[T_0]^2$, where K_0 is the equilibrium constant for the stathmin activation reaction,

$$\alpha(s) = \left[(1 - 2s)^3 + \frac{9}{k}(1 + s) + \beta(s)\right]^{1/3},$$

and

$$\beta(s) = 3\sqrt{\frac{3}{k^3}\left[1 + k^2(1 - 2s)^3 + k(2 + 10s - s^2)\right]}.$$

Because the MT growth velocity v_+ depends on the local tubulin concentration, it follows that a spatial variation in active stathmin concentration leads to a spatial variation in the growth velocity. That is, $[T](x,z) = [T_0] t(s_{on}(x,z))$ and

$$v_+(x,z) = (\kappa_{on}[T](x,z) - \kappa_{off})d, \qquad (14)$$

where $d \approx 0.6$ nm is the effective tubulin dimer size and $\kappa_{on}, \kappa_{off}$ are binding and unbinding rates, respectively. Following Zeitz and Kierfeld (18), we take $\omega_{on} \equiv \kappa_{on}[T_0] = 143 \text{ s}^{-1}$, $\kappa_{off}d = 3.6 \text{ nm s}^{-1}$. Note that the growth velocity is effectively a function of the stathmin concentration under the assumption that the tubulin-stathmin reactions are fast relative to other relevant processes. Experimentally one finds that the average time spent in the growing state, $\langle \tau_+ \rangle = 1/\omega_c$, is a linear function of the growth velocity so that the catastrophe rate also becomes space-dependent,

$$\omega_c(x,z) = \frac{1}{a + bv_+(x,z)}, \qquad (15)$$

for constant coefficients $a = 20$ s and $b = 1.38 \times 10^{10} \text{ s}^2 \text{ m}^{-1}$ (31).

Coupling between active transport and MT growth models

The last component of our model is specifying how we couple the stathmin-regulated MT growth model with the active transport model. Suppose that the MT length distributions $p_\pm$ have reached a steady state before the active transport of membrane-bound signaling molecules. We will assume that the total number N of MTs is fixed and that they are uniformly distributed in the interval $x \in [0,L]$. Setting $p(x,z) = p_+(x,z) + p_-(x,z)$, we have

$$\int_0^R p(x,z)dz = \frac{N}{L}, \qquad (16)$$

and the average MT length at x is

$$\bar{z}(x) = \frac{L}{N}\int_0^R zp(x,z)dz. \tag{17}$$

We then make the identification $\phi(x) = \bar{z}(x)$ for all $0 \le x \le L$.

Finally, there are a few assumptions of the Zeitz-Kierfeld model (18) that need to be highlighted with regard to its incorporation into our active transport model. These authors consider a 1D model consisting of an ensemble of parallel MTs aligned along the z axis, and determine the distribution of MT lengths in response to a Rac1-induced stathmin concentration gradient $S(z)$. In our continuum 2D model, we are assuming that at each point x there is an ensemble of MTs along the lines of Zeitz and Kierfeld (18), which sample the local concentration gradient $S(x,z)$ for the given x. We consider a continuum model, because we can then use analytical and numerical methods from the theory of partial differential equations. However, the validity of a continuum model is based on the assumption that the number of MTs is sufficiently large. In the case of relatively few MTs one would need to consider a stochastic model, in which one keeps track of the growth and shrinkage of individual MTs (see also Mahajan and Athale (17)). One would also have to consider a stochastic version of the active transport model. Another assumption of the Zeitz-Kierfeld model is that the tubulin concentration is either uniform or is regulated by the stathmin concentration via fast tubulin-sequestering. Thus it ignores possible changes in the tubulin concentration due to the polymerization/depolymerization of the MTs; the latter would introduce an effective interaction between the MTs (6). For simplicity, we assume that tubulin-sequestering is the dominant process. A third major assumption is that both the stathmin concentration and MT length distribution have sufficient time to reach steady state before significant turning of the growth cone and consequent changes in the Rac1 distribution along the leading edge. This is reasonable given the fast diffusivity of stathmin (15) and the experimental observation that MT dynamical instabilities are at least an order-of-magnitude faster than translocation speeds of a growth cone (46).

RESULTS

We use a combination of steady-state analysis, perturbation methods (see the Supporting Material), and numerical simulations of the model outlined in Materials and Methods to investigate whether the stathmin-based regulation of MT growth provides a plausible mechanism for establishing a nonuniform concentration of membrane-bound signaling proteins via active transport along the MTs. See the Supporting Material for details of our numerical schemes. Results are based on parameter values listed in Table 1 unless specified otherwise.

Active transport along a polarized MT network generates a polarized concentration of membrane signaling molecules

Suppose that the MTs have the same length ξ so that $\phi(x) = \xi > 0$. The corresponding velocity function is then $v(x,z) = v_0 H(\xi - z)$, where H is the Heaviside function. The steady-state solutions $c(x,z)$ and $u(x)$ satisfy Eqs. 1a and 1b with all time derivatives set to zero, and the jump conditions reduce to

$$c(x,\xi^+) = c(x,\xi^-),$$
$$D\frac{\partial c}{\partial z}(x,\xi^-) - v_0 c(x,\xi^-) = D\frac{\partial c}{\partial z}(x,\xi^+), \tag{18}$$

where $\xi^\pm = \lim_{\epsilon \to 0}[\xi \pm \epsilon], \epsilon > 0$. After imposing the various boundary conditions, we obtain the x-independent solutions

$$c(z) = \begin{cases} c_0 e^{\frac{-v_0}{D}(R-z)}, & \text{if } 0 < z < \xi, \\ c_0 e^{\frac{-v_0}{D}(R-\xi)}, & \text{if } \xi < z < R \end{cases} \tag{19}$$

and

$$u = \frac{k_+}{k_-}c(R) = c_0\frac{k_+}{k_-}e^{-\frac{v_0}{D}(R-\xi)}. \tag{20}$$

The coefficient c_0 is determined by the conservation equation

$$\int_0^L u(x)dx + \int_0^R \int_0^L c(x,z)dxdz = M, \tag{21}$$

where M is the total number of proteins. Hence,

$$c_0 = \frac{M/L}{e^{-v_0(R-\xi)/D}(k_+/k_- + R - \xi + D/v_0) - (D/v_0)e^{-\frac{v_0}{D}R}}.$$

Let us now consider steady-state solutions of the active transport model given by Eqs. 1a and 1b with a nonuniform distribution of MT lengths as specified by an interface function of the form

$$\phi(x) = z_0[1 + \sigma\cos(\pi x/L)]. \tag{22}$$

When σ is small, we can use regular perturbation theory to obtain an approximate solution of the steady-state membrane concentration (see the Supporting Material),

$$u(x) = \frac{k_+ c_0}{k_-}e^{-\frac{v_0}{D}z_R} + \sigma u_1 \cos(\pi x/L) + O(\sigma^2), \tag{23}$$

where $z_R = R - z_0$,

$$u_1 = \frac{A_1(1 + C_1)k_+ c_0}{k_- + D_m\pi^2/L^2}e^{-\frac{v_0}{D}z_R}$$

and

$$A_1 = \frac{v_0 z_0}{D}\frac{1}{1 + \sqrt{\lambda_1}/\rho_1 e^{\sqrt{\lambda_1}z_R} + C_1\left(1 - \sqrt{\lambda_1}/\rho_1\right)e^{-\sqrt{\lambda_1}z_R}},$$

$$C_1 = \frac{D\sqrt{\lambda_1} - \dfrac{k_+ D_m\lambda_1}{k_- + D_m\lambda_1}}{D\sqrt{\lambda_1} + \dfrac{k_+ D_m\lambda_1}{k_- + D_m\lambda_1}}.$$

Here

$$\lambda_1 = \left(\frac{\pi}{L}\right)^2,$$

$$\rho_1 = \frac{-v_0 + \sqrt{v_0^2 + 4D^2\pi^2/L^2}}{2D}.$$

In Fig. 4, we compare the approximate perturbative solution with a numerical solution of the full equations for $\sigma = 0.1, 0.05$. It can be seen that there is good agreement, but the amplitude of the inhomogeneity is small. However, the same type of behavior is obtained as the amplitude σ of the inhomogeneity is increased. This is illustrated in Fig. 5.

A nonuniform distribution of active Rac1 generates a nonuniform distribution of MT lengths

Next we turn to steady-state solutions of the 2D MT/stathmin model given by Eqs. 7, 10, and 11. We first consider the case of a uniform Rac1 distribution, $r_{on}(x) = r_0$, for which we can directly apply the steady-state analysis of Zeitz and Kierfeld (18). Setting $\omega_c = \omega_c(z)$ and $v_+ = v_+(z)$, adding Eqs. 7a and 7b, and setting time-derivatives to zero yields the x-independent steady-state equation ∂z $[v_+(z)p_+(z) - v_-p_-(z)] = 0$. This implies that

$$v_+(z)p_+(z) - v_-p_-(z) \equiv J.$$

The boundary condition at $z = 0, R$ requires that $J = 0$. It follows that

$$p_-(z) = \frac{v_+(z)}{v_-}p_+(z). \tag{24}$$

Substituting Eq. 24 into Eq. 7a gives

$$\frac{\partial v_+(z)p_+(z)}{\partial z} + \left[\frac{\omega_r}{v_-} - \frac{\omega_c(z)}{v_+(z)}\right]v_+(z)p_+(z) = 0.$$

Hence

$$v_+(z)p_+(z) = v_+(0)p_+(0)\exp\left(\int_0^z \lambda(z')dz'\right),$$

where

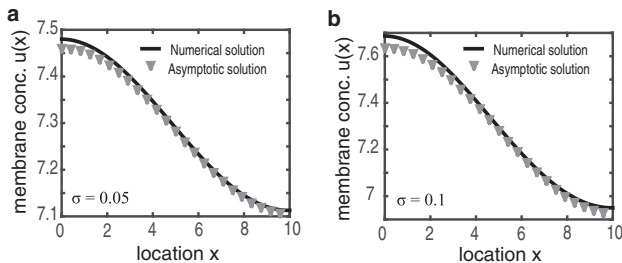$$\lambda(z) = \frac{\omega_r}{v_-} - \frac{\omega_c(z)}{v_+(z)}. \tag{25}$$

FIGURE 4 Numerical solutions of Eqs. 1a and 1b versus perturbative solutions for (a) $\sigma = 0.05$ and (b) $\sigma = 0.1$. Other model parameters are as follows: $R = 10\ \mu m$, $L = 10\ \mu m$, $D = 0.1\ \mu m^2\ s^{-1}$, $D_m = 0.01\ \mu m^2\ s^{-1}$, $k_- = 0.1\ s^{-1}$, $k_+ = 1\ \mu m\ s^{-1}$, $v_0 = 1\ \mu m\ s^{-1}$, and $z_0 = R/2$.
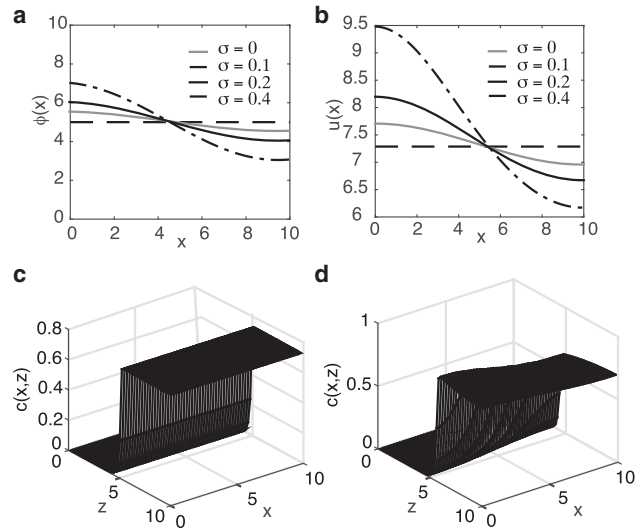
FIGURE 5 Numerical solutions of Eqs. 1a and 1b. (a) Interface function $\phi(x) = 5(1 + \sigma \cos(\pi x/L))$ for various σ. (b) Corresponding steady-state membrane concentration $u(x)$. (c and d) Surface plots of cytosolic concentration $c(x,z)$ for $\sigma = 0.0$ and $\sigma = 0.1$, respectively. Other parameters as in Fig. 4.

It follows that the total density of MTs with length z is

$$p(z) \equiv p_+(z) + p_-(z) = \left(1 + \frac{v_+(z)}{v_-}\right)p_+(z)$$

$$= \mathcal{N}\left(1 + \frac{v_-}{v_+(z)}\right)\exp\left(\int_0^z \lambda(z')dz'\right). \tag{26}$$

The normalization factor $\mathcal{N}$ is determined by Eq. 16, which gives

$$\mathcal{N} = \frac{N}{L}\left[\int_0^R \left(1 + \frac{v_-}{v_+(z)}\right)\exp\left(\int_0^z \lambda(z')dz'\right)dz\right]^{-1}. \tag{27}$$

It remains for us to determine the z dependence of the functions $v_+(z)$ and $\omega_c(z)$ by finding the steady-state solution of the expressions in Eqs. 10a and 10b for stathmin. In the case of a uniform Rac1 concentration, there exists an x independent steady-state solution for S_{off} of the form

$$S_{off}(z) = \Lambda_0\cosh(v_0 z),$$

$$v_0 = \sqrt{\frac{k_{on}}{D_s}}. \tag{28}$$

The coefficient Λ_0 depends on the steady-state boundary condition at the leading edge ($z = R$), where deactivation of stathmin takes place:

$$\frac{D_s}{\delta}\frac{\partial S_{off}}{\partial z}\bigg|_{z=R} = k_{off}r_{on}S_{on}(R) - k_{on}S_{off}(R). \tag{29}$$

Let $S(z) = S_{\text{on}}(z) + S_{\text{off}}(z)$ be the total stathmin concentration at z. Because $S(z)$ evolves according to the 1D steady-state diffusion equation with reflecting boundaries, it follows that $S(z) = S_{\text{tot}} = $ constant. Hence

$$S_{\text{on}}(z) = S_{\text{tot}} - S_{\text{off}}(z) = S_{\text{tot}} - \Lambda_0 \cosh(\nu_0 z). \quad (30)$$

Substituting Eq. 30 into the boundary condition Eq. 29 gives

$$\Lambda_0 = \frac{S_{\text{tot}} k_{\text{off}} r_0}{(D_s/\delta)\nu_0 \sinh(\nu_0 R) + (r_0 k_{\text{off}} + k_{\text{on}})\cosh(\nu_0 R)}. \quad (31)$$

Finally, one can determine the average MT length by substituting for S_{on} into either model of stathmin-MT coupling: Eq. 13 (direct interactions) or Eqs. 14 and 15 (indirect interactions via tubulin-sequestering). For example, in the former case, we have

$$\omega_c(z) = \omega_c^0 + k_c[S_{\text{tot}} - \Lambda_0 \cosh(\nu_0 z)]. \quad (32)$$

Substituting Eq. 32 into the steady-state density of MT lengths, Eq. 26, and using Eq. 25, gives

$$p(z) = \mathcal{N}\left(1 + \frac{v_+}{v_-}\right)\exp\left[\gamma z + \frac{k_c}{v_+}\frac{\Lambda_0}{\nu_0}\sinh(\nu_0 z)\right], \quad (33)$$

where

$$\gamma = \frac{\omega_r}{v_-} - \frac{\omega_c^0 + k_c S_{\text{tot}}}{v_+} \quad (34)$$

and

$$\mathcal{N}\left(1 + \frac{v_+}{v_-}\right) = \frac{N}{L}\left[\int_0^R \exp\left[\gamma z + \frac{k_c}{v_+}\frac{\Lambda_0}{\nu_0}\sinh(\nu_0 z)\right] dz\right]^{-1}.$$

We conclude that for a uniform distribution of active Rac1 within the membrane, the profile of MT lengths in Fig. 3 is $\phi(x) = \bar{z}$ with

$$\bar{z} = \frac{L}{N}\int_0^R z p(z) dz.$$

In Fig. 6 we plot the mean MT length distribution $\bar{z} = \xi$ as a function of S_{tot} for both forms of MT-stathmin interactions, recovering previous results in Zeitz and Kierfeld (18). Note that we use very similar parameter values to those of Zeitz and Kierfeld (18) (see Table 1). Fig. 6 suggests that in the full 2D model, a spatial variation in active Rac1 concentration, $r(x)$, will result in a spatial variation in the mean length $\bar{z} = \bar{z}(x)$ and, hence a spatially varying interface function $\phi(x) = \bar{z}(x)$ for the active transport model.
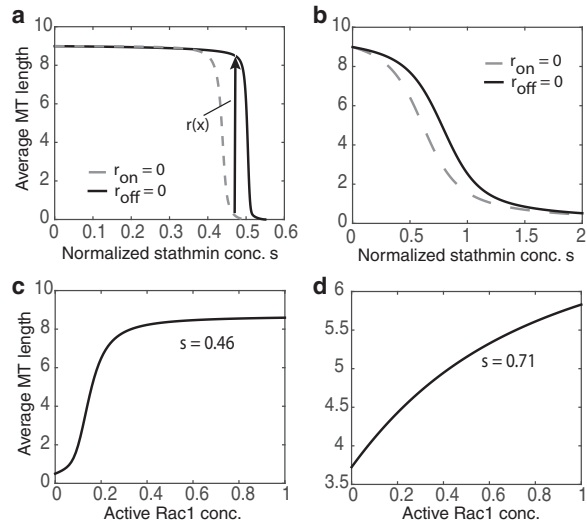
FIGURE 6 Steady-state solutions for the average MT length $\bar{z}$ as a function of the normalized stathmin concentration $s = S_{\text{tot}}/[T_0]$, where $[T_0]$ is the total tubulin concentration, and the active Rac1 concentration for fixed s. (*a* and *c*) Tubulin-sequestering stathmin. (*b* and *d*) Catastrophe-promoting stathmin. For sufficiently large s, the model acts like a switch, jumping from a small $\bar{z}$ in the absence of active Rac1 ($r_0 = 0$) to a large $\bar{z}$ for constitutively active Rac1 ($r_0 = 1$). In our 2D model, we expect a spatial variation in active Rac1 concentration, $r(x)$ to result in a spatial variation in the mean length $\bar{z} = \bar{z}(x)$ and, hence, a spatially varying interface function $\phi(x) = \bar{z}(x)$. Parameters values are taken from Zeitz and Kierfeld (18), where one can find a table listing the various parameters and references to the supporting experimental literature: $v_+ = 0.06\ \mu\text{m s}^{-1}$, $v_- = 0.18\ \mu\text{m s}^{-1}$, $\omega_r = 0.18\ \text{s}^{-1}$, $k_c = 0.005\ \text{s}^{-1}\ \mu\text{M s}^{-1}$, $D_s = 15\ \mu\text{m}^2\ \text{s}^{-1}$, $k_{\text{on}} = 1\ \text{s}^{-1}$, $k_{\text{off}} = 300\ \text{s}^{-1}$, and $\delta = 0.02\ \mu\text{m}$.

Now suppose we have a nonuniform Rac1 concentration given by

$$r_{\text{on}}(x) = r_0 + r_1 \cos(\pi x/L).$$

When r_1 is small, we can again use perturbation theory to obtain an approximate solution of the steady-state stathmin concentration in the cytosol (see the Supporting Material),

$$S_{\text{on}}(x, z) = S_{\text{tot}} - \Lambda_0 \cosh(\nu_0 z) - \epsilon\Lambda_1 \cos(\mu_1 x)\cosh(\nu_1 z),$$

with Λ_0 given by Eq. 31, $\nu_n = \sqrt{k_{\text{on}}/D_s + (n\pi/L)^2}$, and

$$\Lambda_1 = \frac{[S_{\text{tot}} - S_{\text{off}}(0)]k_{\text{off}}}{(D_s/\delta)\nu_1 \sinh(\nu_1 R) + [k_{\text{on}} + r_0 k_{\text{off}}]\cosh(\nu_1 R)}.$$

For catastrophe-promoting stathmin, the numerical solution of the mean length of MTs agrees well with the asymptotic expansion solution we have derived in the Supporting Material (and see Fig. 7). Because of the strongly nonlinear dependence of the MT growth velocity on the active stathmin, it is difficult to find an asymptotic expansion solution of the mean MT length for tubulin-sequestering stathmin.

The numerical solutions of the mean MT length for both tubulin-sequestering stathmin and catastrophe-promoting
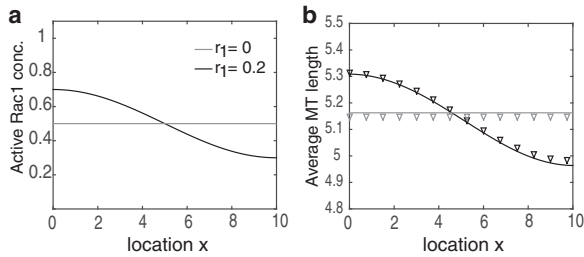
FIGURE 7 Numerical and asymptotic solution of average MT length with catastrophe-promoting stathmin. (*a*) Concentration of active Rac1 $r_{on}(x) = 1 + r_1 \cos(\pi x/L)$ for $r_1 = 0, 0.2$. (*b*) Corresponding steady-state distribution of average MT lengths as a function of membrane coordinate x using numerical simulation (*solid lines*) and perturbation theory (*markers*). The normalized stathmin concentration is $s = S_{tot}/[T_0] = 0.71$. Other parameters are as in Fig. 6.

stathmin are plotted in Fig. 8 for a wider range of r_1 values. In the case of the sinusoidal Rac1 distribution $r_{on}(x) = r_0 + r_1 \cos(\pi x/L)$, the corresponding MT length distribution exhibits only a weak spatial variation even for large-amplitude Rac1 inhomogeneities. This holds for both tubulin-sequestering stathmin and catastrophe-promoting stathmin, and is mainly due to the lateral diffusion of the stathmin in the 2D growth cone. A more significant spatial variation in
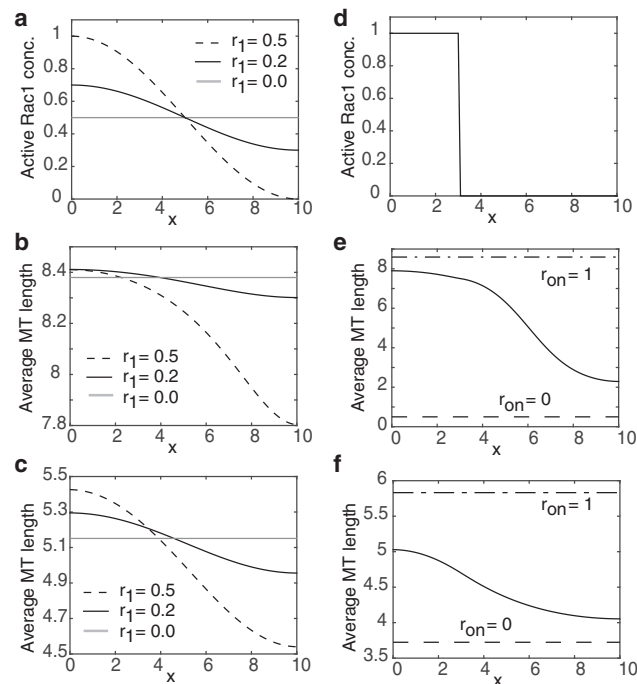

FIGURE 8 Average MT lengths for sinusoidal and piecewise Rac1 concentration profiles. (*a*) Plot of Rac1 distribution $r_{on}(x) = 0.5 + r_1 \cos(\pi x/L)$ for different values of r_1. (*b* and *c*) Corresponding MT length distributions for tubulin-sequestering and catastrophe-promoting stathmin, respectively. (*d*). Plot of piecewise Rac1 distribution. (*e* and *f*) Corresponding MT length distributions for tubulin-sequestering and catastrophe-promoting stathmin, respectively. The normalized stathmin concentration $s = S_{tot}/[T_0] = 0.46$ for tubulin-sequestering stathmin and $s = 0.71$ for catastrophe-promoting stathmin. Other parameters are as in Fig. 5.

MT lengths is obtained using a piecewise Rac1 distribution, $r_{on}(x) = H(3 - x)$, where H is the Heaviside function. Moreover, the mean MT length changes more dramatically when it is regulated by the tubulin-sequestering mechanism rather than the catastrophe-promoting mechanism. This is consistent with the results of the 1D model in Zeitz and Kierfeld (18); see also Fig. 6. However, due to the diffusion of stathmin in the 2D growth cone, the regulation of MT length by Rac1 is weakened compared to the 1D model. As the active Rac1 concentration r_{on} decreases from 1 to 0, the mean MT length decreases with an upper bound smaller than the MT mean length with $r_{on} = 1$ and a lower bound larger than the MT mean length with $r_{on} = 0$.

A nonuniform distribution of active Rac1 generates a polarized concentration of membrane signaling molecules

Recall that the main goal of our modeling study is to investigate to what extent stathmin-regulated MT polarization provides a possible substrate for membrane polarization via the active transport of signaling molecules along the polarized MT network. This can now be investigated by coupling the Rac1-stathmin model of MT length regulation given by Eqs. 7, 10, and 11 with the active transport model of Eqs. 1*a* and *b*, and 2–6. This is achieved by setting the interface function $\phi(z) = \bar{z}(x)$ with $\bar{z}(x)$ defined according to Eq. 17. For the sake of illustration, we consider the piecewise Rac1 distribution. The numerical solution of the resulting steady-state mean MT length distribution is shown in Fig. 9 *a* and the corresponding membrane concentration $u(x)$ is shown in Fig. 9 *b* for tubulin-sequestering stathmin (*solid curves*) and catastrophe-promoting stathmin (*shaded curves*). In both cases, there exists a stable inhomogeneous distribution of the membrane concentration $u(x)$. However, tubulin-sequestering stathmin generates a significantly larger spatial variation in the membrane concentration $u(x)$.
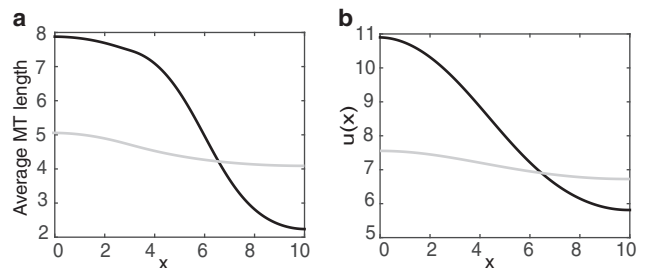

FIGURE 9 Numerical plots of (*a*) mean MT length and (*b*) steady-state membrane concentration $u(x)$ for piecewise active Rac1 distribution. (*Solid curves*) Membrane polarization for MTs regulated by tubulin-sequestering stathmin. The normalized stathmin concentration is $s = S_{tot}/[T_0] = 0.46$. (*Shaded curves*) Membrane polarization for MTs regulated by catastrophe-promoting stathmin. The normalized stathmin concentration is $s = S_{tot}/[T_0] = 0.71$. Other parameters are as in Figs. 5 and 6.

In Fig. 10, we show plots of $u(x)$ with different parameters for tubulin-sequestering stathmin and catastrophe-promoting stathmin, respectively. For tubulin-sequestering stathmin, increasing the shrinkage velocity v_- or reducing the rescue rate ω_r reduces the membrane concentration as well as its spatial variation. We explore how the membrane concentration changes with respect to the growth velocity v_+ by changing the tubulin association rate $\omega_{on} = \kappa_{on}[T_0]$; see Eq. 14. As the tubulin association rate increases, the growth velocity of MTs increases and thus the average MT length also increases, resulting in an increase in membrane concentration. For the catastrophe-promoting stathmin, the membrane concentration is sensitive to the choice of shrinkage velocity, rescue rate ω_r, and catastrophe-promoting constant k_c. It is less sensitive to the catastrophe rate $\omega_c^0 = S_{on} = 0$. Unlike the tubulin-sequestering stathmin mechanism, the degree of spatial variation of $u(x)$ is relatively insensitive to the choice of parameters.

DISCUSSION

In this article, we studied an advection-diffusion model for the active transport of cytosolic signaling proteins along a 2D MT network in a growth cone. The model was coupled to a modified Dogterom-Leibler model of MT growth, with
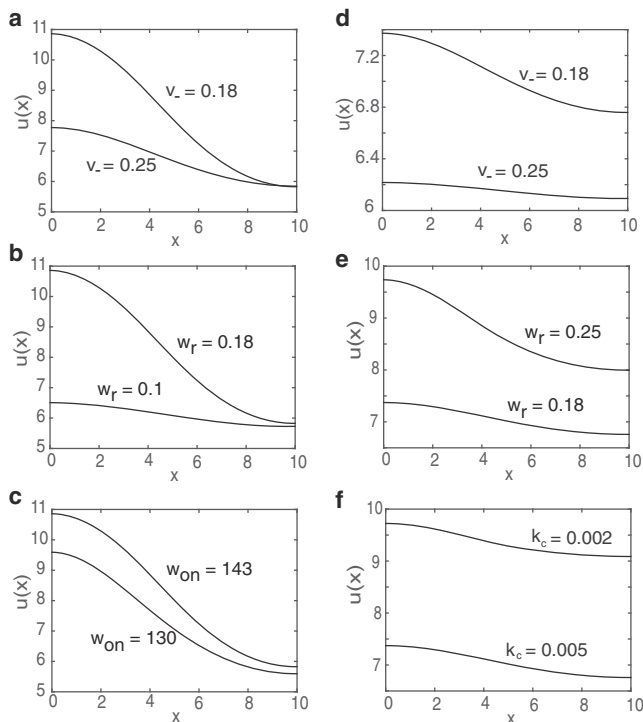
the growth rate and catastrophe rate regulated by stathmin and Rac1 as proposed in Zeitz and Kierfeld (18). The active Rac1 located in the membrane inhibits active stathmin near the membrane, while stathmin in the active state inhibits the growth of MTs via two possible pathways, tubulin-sequestering and catastrophe-promoting. Our model differs from previous studies of the role of active transport in cell polarization, which consider spatial inhomogeneities in the density of MTs in axons (19,20) or actin filaments in budding yeast (21-24). The mechanism in growth cones appears to be different, because MTs nucleate in the cell body, and it is asymmetries in the degree of penetration of MTs into the peripheral zone that contribute to cell polarization.

We first showed that a nonuniform MT network results in a spatially varying concentration of signaling molecules on the membrane. We then explored the MT length distribution under the regulation of stathmin for different choices of the Rac1 distribution on the membrane. For a nonuniform Rac1 distribution, we showed that the MTs grow toward the location with a higher Rac1 concentration for both tubulin-sequestering and catastrophe-promoting stathmin, thus resulting in a polarized distribution of membrane proteins. The spatial variation of the distribution of membrane-bound proteins in the leading edge of the growth cone (degree of membrane polarization) depends on the precise form of the Rac1 distribution and parameters such as the catastrophe-promoting constant and the tubulin association rate. For a piecewise constant Rac1 distribution, tubulin-sequestering stathmin generates more significant membrane polarization than catastrophe-promoting stathmin. However, due to the lateral diffusion of the stathmin in the 2D domain, the spatial variation is smaller than would be expected from the MT length distributions of the 1D model considered by Zeitz and Kierfeld (18). Which of the two stathmin-based regulatory mechanism dominates appears to depend on the pH level, suggesting that perhaps there is some form of pH regulation of stathmin in the growth cone.

One possible extension of our work would be to consider the closed feedback loop of Rac1-Stathmin-MT as proposed in Zeitz and Kierfeld (18), whereby MTs that reach the membrane surface activate Rac1—in particular, to determine whether or not such a feedback mechanism can enhance the inhomogeneity of MT growth, and thus the degree of membrane polarization by counteracting the effects of the lateral diffusion of stathmin. Preliminary simulations (not shown) suggest that this form of feedback does not significantly amplify cell polarization. Another possibility is that the actively transported membrane protein itself provides a source of positive feedback along analogous lines to Cdc42 in budding yeast (21,22). Indeed, Cdc42 could be a candidate signaling molecule.

As highlighted at the end of Methods and Materials, we have assumed that the number of MTs is sufficiently large

FIGURE 10 Parameter dependence of steady-state membrane concentration $u(x)$. (*a–c*) Tubulin-sequestering stathmin: (*a*) shrinkage velocity v_-, (*b*) rescue rate ω_r, and (*c*) tubulin association rate $\omega_{on} = \kappa_{on}[T_0]$. (*d–f*) Catastrophe-promoting stathmin: (*d*) shrinkage velocity v_-, (*e*) rescue rate ω_r, and (*f*) catastrophe promotion constant k_c. The Rac1 distribution is $r_{on} = H(3 - x)$. Other parameters are as in Fig. 5.

so that one can use a deterministic continuum model. In future work we will explore to what extent our results persist when the number of MTs is small. We will then have to consider a stochastic model that keeps track of the growth and shrinkage of individual MTs, as well as the resulting stochastic transport of signaling proteins along the MTs. One possible effect of the noise is that it could counteract the smoothing effects of lateral diffusion, thus allowing more significant membrane polarization.

It would also be interesting to explore how the role of Rac1 in microtubule growth relates to another well-known signaling pathway for growth-cone steering, namely Ca^{2+} (47-49). It is known that extracellular guidance cues cause an asymmetric elevation of Ca^{2+} across the growth cone, which then mediates an imbalance in exocytosis-endocytosis. This in turn redirects lipids, adhesion molecules, and cytoskeletal elements asymmetrically across the growth cone resulting in growth-cone steering. In the case of an attractive (repulsive) cue, Ca^{2+} enhances exocytosis (endocytosis) at the leading edge of the growth cone, resulting in turning the growth cone toward (away from) the extracellular signal. The downstream effects of Ca^{2+} appear to depend on the amplitude of the Ca^{2+} signal. There is also experimental evidence that Rac1 modulates the stimulus-evoked release of Ca^{2+} in growth cones. This occurs via two parallel mechanisms (50): 1) enhancing MT assembly along the lines outlined in our article, which subsequently promotes the spread of the endoplasmic reticulum-based Ca^{2+} release machinery into the growth cone; and 2) increasing so-called reactive oxygen species production, which facilitates inositol 1,4,5-triphosphate (IP_3)-dependent Ca^{2+} release.

Finally, our coupling of protein concentration gradients and MT polarization with active transport could have applications to other related problems in cell biology. In particular, within the context of cell mitosis, spindle MTs are regulated by a concentration gradient of Ran GTPase emanating from the chromosomes (51). This is hypothesized to provide a mechanism for accelerating the search-and-capture of chromosomes by kinetochores.

SUPPORTING MATERIAL

Supporting Materials and Methods and one figure are available at http://www.biophysj.org/biophysj/supplemental/S0006-3495(15)00965-0.

AUTHOR CONTRIBUTIONS

P.C.B. designed the research; P.C.B. and B.X. developed the analysis; B.X. performed the numerical simulations; and P.C.B. and B.X. wrote the article.

ACKNOWLEDGMENTS

REFERENCES

1. Dent, E. W., S. L. Gupton, and F. B. Gertler. 2011. The growth cone cytoskeleton in axon outgrowth and guidance. *Cold Spring Harb. Perspect. Biol.* 3:3.

2. Gordon-Weeks, P. R. 2004. Microtubules and growth cone function. *J. Neurobiol.* 58:70–83.

3. Hoogenraad, C. C., and F. Bradke. 2009. Control of neuronal polarity and plasticity—a renaissance for microtubules? *Trends Cell Biol.* 19:669–676.

4. Poulain, F. E., and A. Sobel. 2010. The microtubule network and neuronal morphogenesis: dynamic and coordinated orchestration through multiple players. *Mol. Cell. Neurosci.* 43:15–32.

5. Mitchison, T., and M. Kirschner. 1984. Dynamic instability of microtubule growth. *Nature.* 312:237–242.

6. Dogterom, M., and S. Leibler. 1993. Physical aspects of the growth and regulation of microtubule structures. *Phys. Rev. Lett.* 70:1347–1350.

7. Gavet, O., S. El Messari, …, A. Sobel. 2002. Regulation and subcellular localization of the microtubule-destabilizing stathmin family phosphoproteins in cortical neurons. *J. Neurosci. Res.* 68:535–550.

8. Poulain, F. E., and A. Sobel. 2007. The "SCG10-LIke Protein" SCLIP is a novel regulator of axonal branching in hippocampal neurons, unlike SCG10. *Mol. Cell. Neurosci.* 34:137–146.

9. Chauvin, S., and A. Sobel. 2015. Neuronal stathmins: a family of phosphoproteins cooperating for neuronal development, plasticity and regeneration. *Prog. Neurobiol.* 126:1–18.

10. Curmi, P. A., S. S. L. Andersen, …, A. Sobel. 1997. The stathmin/tubulin interaction in vitro. *J. Biol. Chem.* 272:25029–25036.

11. Cassimeris, L. 2002. The oncoprotein 18/stathmin family of microtubule destabilizers. *Curr. Opin. Cell Biol.* 14:18–24.

12. Gupta, K. K., C. Li, …, H. V. Goodson. 2013. Mechanism for the catastrophe-promoting activity of the microtubule destabilizer Op18/stathmin. *Proc. Natl. Acad. Sci. USA.* 110:20449–20454.

13. Berzat, A., and A. Hall. 2010. Cellular responses to extracellular guidance cues. *EMBO J.* 29:2734–2745.

14. Watanabe, T., J. Noritake, and K. Kaibuchi. 2005. Regulation of microtubules in cell migration. *Trends Cell Biol.* 15:76–83.

15. Niethammer, P., P. Bastiaens, and E. Karsenti. 2004. Stathmin-tubulin interaction gradients in motile and mitotic cells. *Science.* 303:1862–1866.

16. Yuan, X. B., M. Jin, …, S. Duan. 2003. Signalling and crosstalk of Rho GTPases in mediating axon guidance. *Nat. Cell Biol.* 5:38–45.

17. Mahajan, S., and C. A. Athale. 2012. Spatial and temporal sensing limits of microtubule polarization in neuronal growth cones by intracellular gradients and forces. *Biophys. J.* 103:2432–2445.

18. Zeitz, M., and J. Kierfeld. 2014. Feedback mechanism for microtubule length regulation by stathmin gradients. *Biophys. J.* 107:2860–2871.

19. Hawkins, R. J., O. Bénichou, …, R. Voituriez. 2009. Rebuilding cytoskeleton roads: active-transport-induced polarization of cells. *Phys. Rev. E Stat. Nonlin. Soft Matter Phys.* 80:040903.

20. Bressloff, P. C., and B. Xu. 2015. Stochastic active-transport model of cell polarization. *SIAM J. Appl. Math.* 75:652–678.

21. Wedlich-Soldner, R., S. C. Wai, …, R. Li. 2004. Robust cell polarity is a dynamic state established by coupling transport and GTPase signaling. *J. Cell Biol.* 166:889–900.

22. Marco, E., R. Wedlich-Soldner, …, L. F. Wu. 2007. Endocytosis optimizes the dynamic localization of membrane proteins that regulate cortical polarity. *Cell.* 129:411–422.

23. Layton, A. T., N. S. Savage, …, D. J. Lew. 2011. Modeling vesicle traffic reveals unexpected consequences for Cdc42p-mediated polarity establishment. *Curr. Biol.* 21:184–194.

24. Jilkine, A., and L. Edelstein-Keshet. 2011. A comparison of mathematical models for polarization of single eukaryotic cells in response to guided cues. *PLOS Comput. Biol.* 7:e1001121.

25. Walker, R. A., E. T. O'Brien, …, E. D. Salmon. 1988. Dynamic instability of individual microtubules analyzed by video light microscopy: rate constants and transition frequencies. *J. Cell Biol.* 107:1437–1448.

26. Janson, M. E., and M. Dogterom. 2004. Scaling of microtubule force-velocity curves obtained at different tubulin concentrations. *Phys. Rev. Lett.* 92:248101.

27. Drechsel, D. N., A. A. Hyman, …, M. W. Kirschner. 1992. Modulation of the dynamic instability of tubulin assembly by the microtubule-associated protein tau. *Mol. Biol. Cell.* 3:1141–1154.

28. Gildersleeve, R. F., A. R. Cross, …, R. C. Williams, Jr. 1992. Microtubules grow and shorten at intrinsically variable rates. *J. Biol. Chem.* 267:7995–8006.

29. Pryer, N. K., R. A. Walker, …, E. D. Salmon. 1992. Brain microtubule-associated proteins modulate microtubule dynamic instability in vitro. Real-time observations using video microscopy. *J. Cell Sci.* 103:965–976.

30. Nakao, C., T. J. Itoh, …, N. Mori. 2004. Modulation of the stathmin-like microtubule destabilizing activity of RB3, a neuron-specific member of the SCG10 family, by its N-terminal domain. *J. Biol. Chem.* 279:23014–23021.

31. Janson, M. E., M. E. de Dood, and M. Dogterom. 2003. Dynamic instability of microtubules is regulated by force. *J. Cell Biol.* 161:1029–1034.

32. Jourdain, L., P. Curmi, …, M.-F. Carlier. 1997. Stathmin: a tubulin-sequestering protein which forms a ternary T2S complex with two tubulin molecules. *Biochemistry.* 36:10817–10821.

33. Honnappa, S., B. Cutting, …, M. O. Steinmetz. 2003. Thermodynamics of the Op18/stathmin-tubulin interaction. *J. Biol. Chem.* 278:38926–38934.

34. Amayed, P., D. Pantaloni, and M.-F. Carlier. 2002. The effect of stathmin phosphorylation on microtubule assembly depends on tubulin critical concentration. *J. Biol. Chem.* 277:22718–22724.

35. Howell, B., N. Larsson, …, L. Cassimeris. 1999. Dissociation of the tubulin-sequestering and microtubule catastrophe-promoting activities of oncoprotein 18/stathmin. *Mol. Biol. Cell.* 10:105–118.

36. Beller, J. A., B. Kulengowski, …, D. M. Snow. 2013. Comparison of sensory neuron growth cone and filopodial responses to structurally diverse aggrecan variants, in vitro. *Exp. Neurol.* 247:143–157.

37. Reed, M. C., S. Venakides, and J. J. Blum. 1990. Approximate traveling waves in linear reaction-hyperbolic equations. *SIAM J. Appl. Math.* 50:167–180.

38. Friedman, A., and B. Hu. 2007. Uniform convergence for approximate traveling waves in linear reaction-hyperbolic systems. *Indiana Univ. Math. J.* 56:2133–2158.

39. Newby, J. M., and P. C. Bressloff. 2010. Quasi-steady state reduction of molecular motor-based models of directed intermittent search. *Bull. Math. Biol.* 72:1840–1866.

40. Bressloff, P. C., and J. Newby. 2011. Quasi-steady-state analysis of two-dimensional random intermittent search processes. *Phys. Rev. E Stat. Nonlin. Soft Matter Phys.* 83:061139.

41. Heinrich, R., and T. A. Rapoport. 2005. Generation of nonidentical compartments in vesicular transport systems. *J. Cell Biol.* 168:271–280.

42. Dighe, S. A., and K. G. Kozminski. 2014. Secretory vesicles deliver Cdc42p to sites of polarized growth in *S. cerevisiae. PLoS One.* 9:e99494.

43. Tojima, T. 2012. Intracellular signaling and membrane trafficking control bidirectional growth cone guidance. *Neurosci. Res.* 73:269–274.

44. Brown, G. C., and B. N. Kholodenko. 1999. Spatial gradients of cellular phospho-proteins. *FEBS Lett.* 457:452–454.

45. Lipkow, K., and D. J. Odde. 2008. Model for protein concentration gradients in the cytoplasm. *Cell. Mol. Bioeng.* 1:84–92.

46. Geraldo, S., and P. R. Gordon-Weeks. 2009. Cytoskeletal dynamics in growth-cone steering. *J. Cell Sci.* 122:3595–3604.

47. Tojima, T., J. H. Hines, …, H. Kamiguchi. 2011. Second messengers and membrane trafficking direct and organize growth cone steering. *Nat. Rev. Neurosci.* 12:191–203.

48. Tojima, T., R. Itofusa, and H. Kamiguchi. 2014. Steering neuronal growth cones by shifting the imbalance between exocytosis and endocytosis. *J. Neurosci.* 34:7165–7178.

49. Sutherland, D. J., Z. Pujic, and G. J. Goodhill. 2014. Calcium signaling in axon guidance. *Trends Neurosci.* 37:424–432.

50. Zhang, X.-F., and P. Forscher. 2009. Rac1 modulates stimulus-evoked Ca^{2+} release in neuronal growth cones via parallel effects on microtubule/endoplasmic reticulum dynamics and reactive oxygen species production. *Mol. Biol. Cell.* 20:3700–3712.

51. Caudron, M., G. Bunt, …, E. Karsenti. 2005. Spatial coordination of spindle assembly by chromosome-mediated signaling gradients. *Science.* 309:1373–1376.